Available online at www.sciencedirect.com
SCIENCE DIRECT
Polymer 46 (2005) 3884–3894
polymer
www.elsevier.com/locate/polymer

# Mechanical response of dibenzyl-based polyurethanes with diol chain extension

C. Prisacariu[a], C.P. Buckley[b,*], A.A. Caraculacu[a]

[a]*Petru Poni Institute of Macromolecular Chemistry of the Romanian Academy, Aleea Grigore Ghica Voda, Nr. 41 A, Iasi 700487, Romania*
[b]*Department of Engineering Science, University of Oxford, Parks Road, Oxford OX1 3PJ, UK*

Received 1 September 2004; received in revised form 11 March 2005; accepted 18 March 2005

**Abstract**

A systematic investigation was made of the effects of varying hard and soft segment chemistry, crosslinking and preparation procedures, on the mechanical response of melt-cast polyurethane elastomers. In particular, two hard segments were compared, based on the diisocyanates: 4,4′-methylene bis(phenyl isocyanate) (MDI) and 4,4′-dibenzyl diisocyanate (DBDI). Rotation around the central $–CH_2–CH_2–$ bridge in DBDI allows alignment of aromatic rings and hence crystallization within the hard phase, which is not available with MDI in melt-cast polyurethanes. Thus, new polymers were achieved, with a controlled ordering of copolymer hard segment blocks on the macromolecular chain. Wide angle X-ray diffraction of the as-moulded polymers revealed the presence of crystallinity in some cases, in the DBDI-based PU materials. Mechanical tests included load–unload cycles at constant rate of extension, with measurement of hysteresis and strain recovery, and stress relaxation tests. The presence of DBDI hard segments instead of MDI led systematically to increases in: the input strain energy to a given elongation, hysteresis and residual strain under cyclic loading, and stress relaxation. The results were interpreted in terms of a physically-based constitutive model framework previously proposed. This revealed that the observed effects of varying hard segment could all be explained by the hard domains having a higher flow stress in the presence of DBDI relative to MDI, associated with increased hydrogen bonding in DBDI-based polymers, which is enhanced in some cases by hard segment crystallinity. Materials with mixed MDI and DBDI hard segments were found to give the optimum combination of high input strain energy, but minimum residual strain, compared to equivalent materials based on MDI or DBDI alone.


*Keywords:* Polyurethanes; Diisocyanates; Physical–mechanical properties

## 1. Introduction

The main goal of this study is to investigate the mechanical performance of novel polyurethane (PU) elastomers and films derived from complex dibenzyl hard segments, which are characterized by different packing structures in the PU hard domains [1–4]. The conformational mobility of 4,4′-dibenzyl diisocyanate (DBDI) (Fig. 1) causes an unusually wide range of mechanical, physical and chemical properties, associated with the possibility of pronounced phase separation into a domain–matrix morphology, and with a higher tendency to crystallization and self-association by hydrogen bonding [1].

The more usual 4,4′-methylene bis(phenyl isocyanate) (MDI) hard segment introduces into the polyurethane chain the rigid $–∅–CH_2–∅–$ moiety, concentrated in the hard domains. In contrast, as reported previously [5,6], when DBDI is chosen as hard segment, the $–∅–CH_2–CH_2–∅–$ moiety makes possible a change in the geometry of the hard segments as a result of internal rotation around the $–CH_2–CH_2–$ ethylene bridge. This difference is shown in Fig. 1. By synthesising elastomers based on one or both of MDI or DBDI, it has become possible to study the effects of varying hard phase crystallinity.

In the present study, a range of PU elastomers containing such hard segments was prepared, and their mechanical properties compared. Thus they were based on the diisocyanates: MDI (here labeled PUs of type M), DBDI (PUs of type D), or in some cases an equimolar mixture of

* Corresponding author. Tel.: +44 1865 273156; fax: +44 1865 273906.
*E-mail address:* paul.buckley@eng.ox.ac.uk (C.P. Buckley).

0032-3861/$ - see front matter © 2005 Elsevier Ltd. All rights reserved.
doi:10.1016/j.polymer.2005.03.046

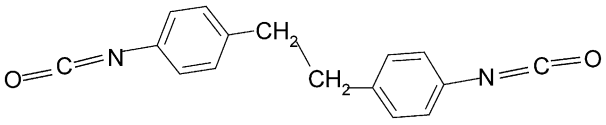

DBDI

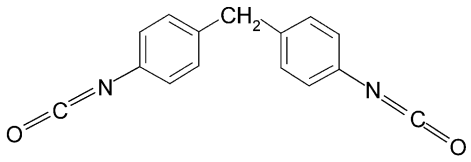

MDI

Fig. 1. Schematic of 4,4′-dibenzyl diisocyanate (DBDI) and comparison to 4,4′-methylene bis(phenyl isocyanate) (MDI).

MDI and DBDI (PUs of type C), as listed in Table 1. Some results showing the effects of using a mixture of the diisocyanates were already reported recently [7]. The range of polymers was designed also to reveal the roles of choice of macrodiol (MD) and of chain extender (CE) in determining the performance as an elastomer. The soft segment MD was either polytetrahydrofuran (PTHF) or poly(ethylene adipate) (PEA) of molar mass $2000 \pm 50$. The CE used in the synthesis was ethylene glycol (EG), 1,4-butanediol (BG) or diethylene glycol (DEG).

In view of the better elastomeric properties produced, in most cases reactive PU with a small excess of NCO groups was prepared, by using a deficit of CE with molar concentrations such as DBDI:PTHF:DEG = 3:1:1.73, giving isocyanic index $I = 110$ [7]. In this case the synthesis was complete only when there was total consumption of isocyanate excess by ambient humidity, leading to significant macromolecular chain extension by urea group linkages and (to a much smaller degree [2]) by allophanate crosslinks. In the single case of polymer PU5 (see Table 1) stoichiometric proportions were used (isocyanic index $I = 100$) and therefore this route to further chain extension in the presence of air humidity was not available, producing a polymer without urea groups and possibly without crosslinks: molar proportions used in this synthesis were: DBDI:PTHF:DEG = 3:1:2 [1].

To investigate how the PU structure determines the mechanical performance of the materials as elastomers, a programme of cyclic tensile tests was carried out on the whole range of polymers synthesized. Properties of particular interest were the strain energy input, and the strain energy recovery and strain recovery on unloading. In some cases these experiments were supplemented by stress relaxation tests. Wide angle X-ray diffraction (WAXD) was employed to compare the levels of hard segment crystallinity.

A general framework for constitutive modeling of solid polymers proposed previously [8] proved useful for interpreting the mechanical property differences observed. Specifically, the stress contributions from hard phase viscoplasticity and soft phase elasticity could be identified separately, and related to the details of PU chemical structure [9,10].

## 2. Experimental

### 2.1. Synthesis

(a) For synthesis of the simple typical copolyurethane elastomers from a single diisocyanate (PUs type M or D) (Table 1) the following procedure was followed. For example, in the case of polymers with molar ratios DI:MD:CE = 4:1:2.64, 100 g (0.05 mol of macrodiol PEA or PTHF, respectively) was dehydrated by stirring at 110 °C under vacuum (< 1 mm Hg) for 2 h. Fifty grams (0.2 mol) of MDI in the case of PUs type M or respectively 52.8 g (0.2 mol) of DBDI for PUs type D, was added to the anhydrous macrodiol with intense mixing, and vacuum was restored. After 30 min of mixing under vacuum at 100 °C the temperature was reduced to 90 °C and vacuum was removed. A prepolymer was obtained with final NCO groups in a mixture with the excess of isocyanate. Then 0.132 mol of CE was added quickly with rapid stirring. The mixing was continued for a maximum of 30–40 s. After addition of the CE the prepolymer melt was poured into a sheet mould and cured by heating for 24 h at 110 °C. In the case of sheets up to 2 mm thick, PUs prepared with stoichiometric deficit of CE ($I = 110$) were postcured by holding for 2 weeks under ambient humidity, so as to obtain a further increase of the molecular weight as a result of the NCO excess transforming into urea linkages and allophanate crosslinks. The polyurethanes PU1-4 and 6–17 mentioned in Table 1 were synthesized in this manner, by using the reactant molar ratios indicated in the table.

(b) Copolyurethane elastomers of type C (PU18 and 19 in Table 1), containing diisocyanates MDI and DBDI randomly distributed, were synthesized starting from PEA or from PTHF as in case (a). The only difference was that in both cases in the prepolymer synthesis a melt mixture of DBDI and MDI was used in equal molar proportions, and was introduced into the anhydrous macrodiol. The remaining synthesis steps, the chain extension, curing and postcuring, were performed in the same manner as in procedure (a).

### 2.2. Mechanical tests

The polymers in Table 1, in the form of films prepared as described above, were subjected to uniaxial tensile tests at constant nominal strain-rate. In addition, to investigate mechanical hysteresis, cyclic tensile tests were carried out, cycling between a fixed strain limit and zero load, with the same magnitude of strain-rate for loading and unloading. Furthermore, to reveal the time-dependent contribution to

Table 1
The family of PU elastomers studied, based on the two di-isocyanates DBDI and MDI

| PU# | PU type | PU structure | | | | | $E_{1C}$ (MJ m$^{-3}$) | $E^*_{2C}$ (%) | $E^*_{1R}$ (%) | $E^*_{2R}$ (%) |
|---|---|---|---|---|---|---|---|---|---|---|
| | | DI | MD | CE | DI:MD:CE | $I$ % | | | | |
| 1 | D | DBDI | PTHF | DEG | 1.5:1:0.38 | 110 | 8.00 | 77.8 | 50.3 | 48.8 |
| 2 | D | DBDI | PTHF | DEG | 2.27:1:1.065 | 110 | 14.3 | 62.5 | 31.1 | 31.0 |
| 3 | D | DBDI | PTHF | DEG | 3:1:1.73 | 110 | 23.1 | 52.2 | 18.9 | 18.9 |
| 4 | D | DBDI | PTHF | DEG | 4:1:2.64 | 110 | 25.3 | 48.0 | 16.6 | 17.0 |
| 5 | D | DBDI | PTHF | DEG | 3:1:2 | 100 | 20.9 | 51.3 | 17.7 | 18.0 |
| 6 | D | DBDI | PEA | DEG | 3:1:1.73 | 110 | 24.0 | 53.6 | 15.6 | 15.0 |
| 7 | M | MDI | PTHF | DEG | 3:1:1.73 | 110 | 19.0 | 63.8 | 39.1 | 39.0 |
| 8 | M | MDI | PEA | DEG | 3:1:1.73 | 110 | 16.3 | 72.8 | 41.7 | 38.1 |
| 9 | D | DBDI | PEA | BG | 3:1:1.73 | 110 | 41.7 | 32.3 | 16.7 | 11.0 |
| 10 | D | DBDI | PTHF | BG | 3:1:1.73 | 110 | 25.3 | 40.9 | 14.2 | 14.0 |
| 11 | M | MDI | PEA | BG | 3:1:1.73 | 110 | 27.2 | 60.9 | 25.3 | 26.1 |
| 12 | D | DBDI | PEA | EG | 3:1:1.73 | 110 | 41.8 | 33.3 | 10.2 | 13.8 |
| 13 | M | MDI | PEA | EG | 3:1:1.73 | 110 | 21.7 | 62.7 | 33.3 | 33.0 |
| 14 | D | DBDI | PEA | EG | 4:1:2.64 | 110 | 46.6 | 40.9 | 11.5 | 12.2 |
| 15 | M | MDI | PEA | EG | 4:1:2.64 | 110 | 30.4 | 64.6 | 17.6 | 20.2 |
| 16 | D | DBDI | PTHF | EG | 4:1:2.64 | 110 | 41.1 | 36.2 | 10.2 | 10.8 |
| 17 | M | MDI | PTHF | EG | 4:1:2.64 | 110 | 30.6 | 63.2 | 38.9 | 35.2 |
| 18 | C | DBDI+MDI | PEA | EG | 2:2:1:2.64 | 110 | 40.1 | 55.3 | 15.7 | 15.7 |
| 19 | C | DBDI+MDI | PTHF | EG | 2:2:1:2.64 | 110 | 35.7 | 50.2 | 27.9 | 25.5 |

Samples were prepared with systematic variations in diisocyanate (DI), macrodiol (MD) and chain extender (CE). $I$ (isocyanic index %) $= 100 \times [NCO]/([OH]_{MD} + [OH]_{CE})$. Molar ratios were as given in column 6. Strain energy input (at 300% elongation) and strain energy recovery (on unloading from 300% elongation) were measured in cyclic tensile tests at a nominal strain-rate of $3.1 \times 10^{-2}$ s$^{-1}$. Asterisks denote that input energy on the second cycle $E^*_{2C}$ and recovered energies on first and second cycles $E^*_{1R}$ and $E^*_{2R}$ are expressed as percentages of the input energy on the first cycle $E_{1C}$.

stress, some tensile stress relaxation tests were conducted: these included both single strain-step experiments and interrupted constant strain-rate experiments. Test specimens were cut from films using dimensions given in ASTM D1708, i.e. a dumbbell-shaped specimen with a length 53 mm between shoulders, a gauge length of 20 mm (on which the strain was measured), a width of 5.8 mm, and a thickness of 0.3 up to 2 mm. The stress–strain data on these specimens presented here were obtained using an Instron 4204 Testing Machine or Schopper MZ Gip Testing Machine, at room temperature ($T \approx 25\,^{\circ}C$). Strain was measured manually from the movement of fiducial marks or obtained from grip displacement, after using video images of the gauge length to correct for nonuniform strain outside the gauge length. True stress was deduced from nominal stress by assuming incompressibility.

## 3. Results and discussion

### 3.1. Tensile test results

Their performance as elastomers, for the entire series of polymers listed in Table 1, was assessed by means of a series of cyclic tensile tests, at a constant nominal strain-rate of $3.1 \times 10^{-2}\,s^{-1}$, cycling between 300% elongation and zero load. From these tests, the initial input strain energy density $E_{1C}$ was computed as the area under the first cycle loading curve of nominal stress versus nominal strain up to the elongation limit of 300%. The calculation was repeated for the corresponding quantity for the second load cycle: $E_{2C}$. Similarly, recovered energy densities $E_{1R}$ and $E_{2R}$ were computed as the areas under the unloading curves for first and second cycles, respectively. The areas were measured on paper copies of the curves, using a digital planimeter. In the present paper, $E_{2C}$, $E_{1R}$ and $E_{2R}$ are expressed as fractions of the initial input energy density $E_{1C}$, and denoted as such by an asterisk. The fractional energy dissipated on each cycle was expressed as the fractional hysteresis energy density on first and second cycles, obtained from the expressions:

$$E^*_{1H} = 1 - E^*_{1R} \quad (1)$$

$$E^*_{2H} = E^*_{2C} - E^*_{2R} \quad (2)$$

Comparing successive load–unload cycles, it was found that irreversible changes to the stress–strain response were confined essentially to the first loading cycle. In subsequent cycles the load–unload stress–strain curves remained almost unchanged. For example, it may be seen from Table 1 that the recovered energies in first and second cycles are equal in most cases, to a good approximation. Similarly, increasing the time interval between the end of one unloading cycle and the start of the next, from a few seconds to several hours (up to 24 h), had no sensible effect on the measured recoverable strain energy. This was in contrast to the input energy, which was clearly dependent on both the previous strain history and the relaxation time between loading cycles [1]. Results are summarized in Table 1. Data for materials PU14–PU19 were presented previously [7], but are included here for comparison to the new data.

Fig. 2 shows the dependence of $E_{1C}$ and $E^*_{1R}$ on the equivalent hard segment urethane group concentration in PUs of structure DEG–PTHF–DBDI (PU1–PU4 in Table 1). As may be seen, $E_{1C}$ increases with increase in concentration of the hard segment urethane groups, reflecting the increase in concentration of hydrogen bonds. In contrast, the fractional recovered energy $E^*_{1R}$ decreases, revealing that the increase in $E_{1C}$ is associated with increased plastic dissipation of energy, presumably resulting from stress-induced breakdown of the hydrogen bonds.

Comparing the DBDI and MDI based polyurethanes of different recipes in Table 1, it is clear that, in recipes otherwise identical (same MD and CE, and equal hard segment molar concentration) the DBDI based PUs display a substantially higher input energy density $E_{1C}$ and lower fractional energy recovery $E^*_{1R}$ than the corresponding MDI based PUs. This applies for all MD/CE combinations studied: PTHF–DEG (compare PU3 with PU7); PEA–DEG (compare PU6 with PU8); PEA–BG (compare PU9 with PU11); PEA–EG (compare PU12 with PU13 and PU14 with PU15); PTHF–EG (compare PU16 with PU17). These findings are summarized in Table 2, where the percentage excess of $E_{1C}$ of the DBDI-based PUs over the MDI-based PUs is shown. A further interesting observation from Table 1 is that, when an equimolar mixture of DBDI + MDI is used for the hard segments, the values of $E_{1C}$ and $E^*_{1R}$ obtained are intermediate between those obtained for the corresponding recipes with either DBDI or MDI alone (consider the families of materials PU14/PU15/PU18 and PU16/PU17/

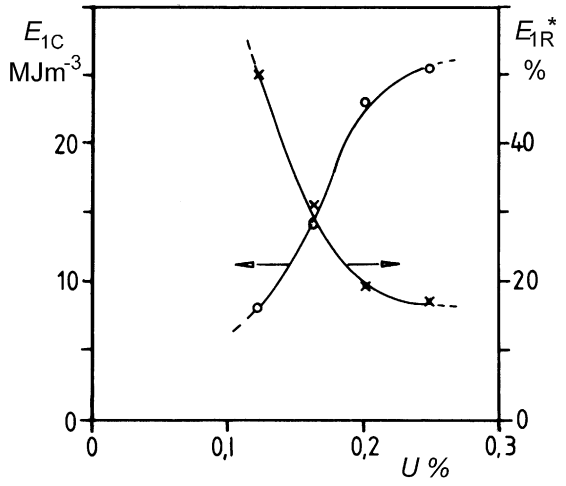


Fig. 2. Variations of input strain energy at 300% elongation $E_{1C}$, and first cycle recovered strain energy $E^*_{1R}$, with concentration $U$ of urethane groups (expressed as equivalent urethanic groups/100 g PU), in the case of a PU system based on DBDI–$PTHF_{2000}$–DEG (polymers PU1–PU4).

Table 2
The increase of strain energy input $E_{1C}$ for DBDI-based PUs over corresponding MDI-based PUs, for various combinations of macrodiol and chain extender

| Polymers compared | MD | CE | Relative $E_{1C}$ increase % |
|---|---|---|---|
| PU7 (MDI) and PU3 (DBDI) | PTHF | DEG | 21.6 |
| PU8 (MDI) and PU6 (DBDI) | PEA | DEG | 47.2 |
| PU11 (MDI) and PU9 (DBDI) | PEA | BG | 53.3 |
| PU13 (MDI) and PU12 (DBDI) | PEA | EG | 92.6 |
| PU15 (MDI) and PU14 (DBDI) | PEA | EG | 53.2 |
| PU17 (MDI) and PU16 (DBDI) | PTHF | EG | 34.3 |

From the data in Table 1.

PU19). Finally, comparison of results for PU5 (DBDI–PTHF–DEG, $I=100$) and PU3 (DBDI–PTHF–DEG, $I=110$) reveals the effects of PU chain structure modification, with the appearance in PU3 of new urea groups and possible formation of some allophanate branching, in the presence of humidity when there is an isocyanate excess. PU3 has a larger input strain energy $E_{1C}$ but also a higher recovery of energy $E^*_{1R}$ than PU5.

The influence of hard segment type on recoverability of energy and strain was examined more closely by means of single-cycle load–unload tensile tests conducted to a range of maximum elongations at a nominal strain-rate of $4.2\times10^{-3}\,s^{-1}$, on a group of three PU materials with equivalent recipes, differing only in the choice of hard segment: PU17 (MDI), PU16 (DBDI) and PU19 (DBDI+MDI). In every case the macrodiol was PTHF and the chain extender was EG, and molar ratios were 4:1:2.64. Results are shown in Figs. 3–5. The influences of hard segment structure on $E_{1C}$ and hysteresis, already referred to, can clearly be seen by eye by comparing Figs. 3–6.

Values of residual elongation after one load–unload

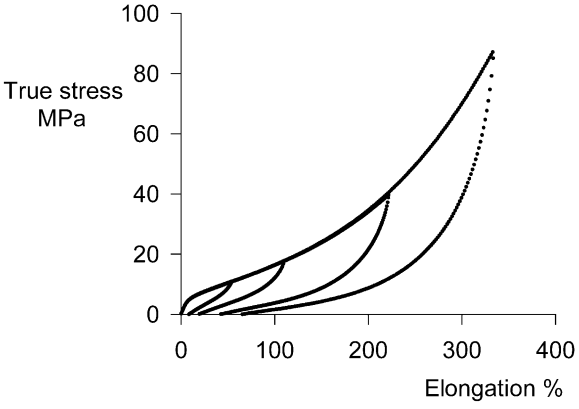


Fig. 3. Tensile load/unload cycles for a type M polymer: PU17 (MDI–PTHF–EG, $I=110$). Nominal extension rate was $0.0042\,s^{-1}$. Each cycle was obtained with a different specimen.

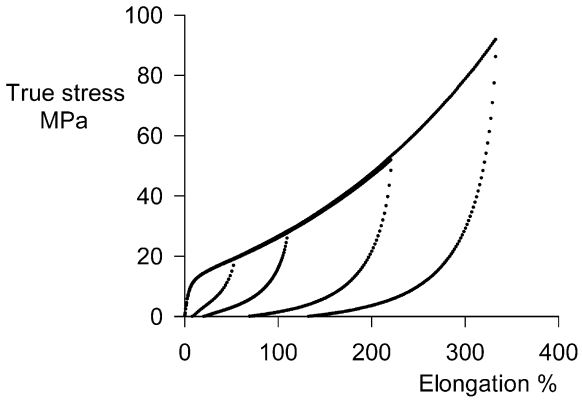


Fig. 4. As Fig. 3, but for type D polymer: PU16 (DBDI–PTHF–EG, $I=110$).

cycle, as obtained from the data in Figs. 3–5, are shown as functions of maximum elongation in Fig. 6. It is interesting to note that, while polymer C occupies an intermediate position relative to M and D in terms of $E_{1C}$ and $E^*_{1R}$, it gives the lowest residual elongation. Fig. 7 shows a comparison of stress–strain curves at this strain-rate for the three PUs, revealing differences in the shapes of the curves.

### 3.2. Stress relaxation

As is widely known, PU elastomers are not perfectly elastic. Thus, when deformation is held constant, the induced stress relaxes gradually. Fig. 8 shows example data, for stress relaxation over 100 h, for PU9 stretched to 300% elongation. It also reveals that over the range shown there is a linear dependence of stress on the logarithm of time, as expressed by Eq. (3).

$$\sigma = \sigma_o - a \log t \tag{3}$$

where $\sigma_o$ and $a$ are constants for a given material. This relation was found to hold for all the materials tested.

Values of percentage stress relaxation, 10 min after straining to 300% elongation at $3.1\times10^{-2}\,s^{-1}$, are

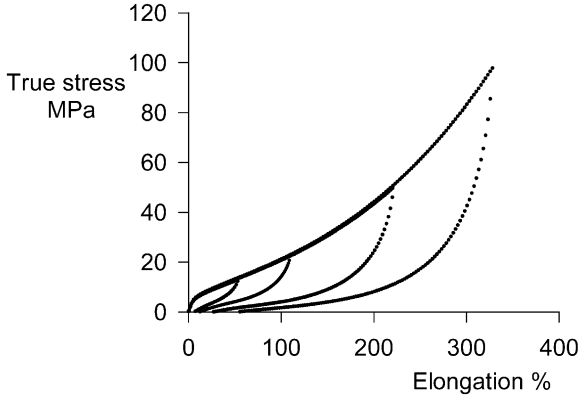


Fig. 5. As Fig. 3, but for type C polymer: PU19 (DBDI+MDI–PTHF–EG, $I=110$).

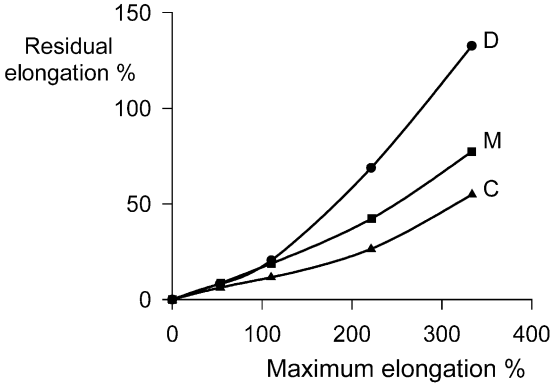


Fig. 6. Residual elongation from one load–unload cycle at nominal strain-rate 0.0042 $s^{-1}$, from the data in Figs. 3–5: comparison of polymers of types M, D and C.

collected in Table 3 for several of the PUs studied, together with the initial nominal stress on reaching 300% elongation $\sigma_{300\%}$. Also shown, for comparison, are the values of first and second cycle hysteresis $E^*_{1H}$ and $E^*_{2H}$ and the residual elongation after unloading from 300% elongation.

The measured values of percent relaxation over 10 min at 300% elongation were found to lie in the range 17–21% in the case of DBDI based PUs, which may be compared with the range 16–24% mentioned by Abouzahr and Wilkes for similar MDI based polyurethane elastomers [11]. As may be seen, the range of stress relaxation for the DBDI and MDI based PU do not differ greatly. Nevertheless, some interesting differences are visible in Table 3. Comparing the results for PU9 and PU11, it may be seen that there is an increase of 14% in stress relaxation when the MDI hard segment is replaced by DBDI, for the same MD/CE combination and urethane group concentration. This is consistent with the increase in residual elongation and hysteresis also shown in Table 3. This table also shows some influence of changing the MD (10% increase in stress relaxation from PTHF to PEA) or the CE (13% increase from BG to DEG), when DBDI was the hard segment. But it is interesting to note that these increases do not correlate

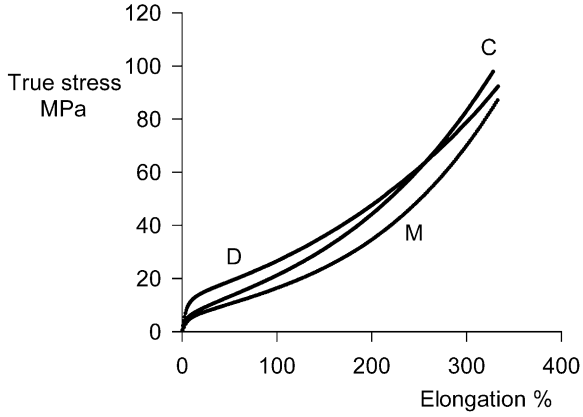


Fig. 7. Comparison of stress–strain curves for the polymers of types M, D and C from Figs. 3–5, during loading at nominal strain-rate 0.0042 $s^{-1}$.

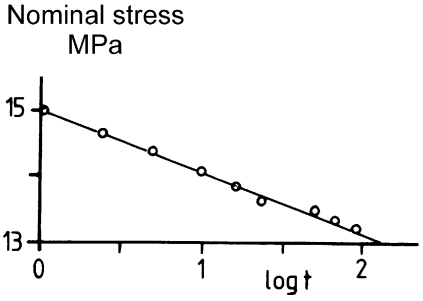


Fig. 8. Stress relaxation of PU 9 (DBDI–PEA–BG, $I=110$) following 300% elongation at nominal strain-rate $3.1\times10^{-2}$ $s^{-1}$. Time $t$ is expressed in hours.

with increases in residual elongation or hysteresis. Other factors are at work here, including the fact that use of DEG as chain-extender inhibits crystallization of the DBDI (see below).

Further tensile stress relaxation tests were conducted by interrupting constant strain-rate tests (again $3.1\times10^{-2}$ $s^{-1}$) at intervals of 25% elongation, to observe the relaxation of stress at constant strain over 10 min, before resuming extension. Sample results are shown in Figs. 9 and 10, where materials based on DBDI and MDI may be compared (PU9 and PU11). In both cases, the stress–strain curve for continuous straining is included for comparison. A common pattern of behaviour can be seen. When straining is resumed after stress relaxation for 10 min, the stress rises rapidly before continuing a steady increase with strain, resuming approximately the original curve. The fact that the stress–strain curves for continuous straining lie slightly below the corresponding envelope curves for the interrupted tests, is believed to reflect a small degree of adiabatic heating in the continuous tests. The nominal strain-rate employed ($3.1\times10^{-2}$ $s^{-1}$) is at the upper end of the range where isothermal conditions are likely to apply in the testing of an elastomer

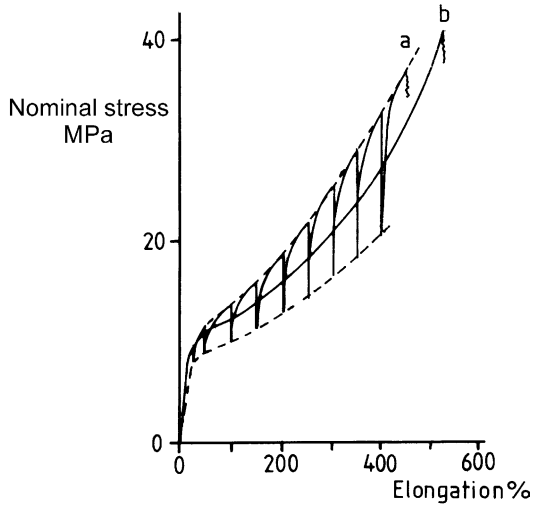


Fig. 9. Stress–strain curves for type D polymer PU9 (DBDI–PEA–BG, $I=110$) at nominal strain-rate $3.1\times10^{-2}$ $s^{-1}$: (a) interrupted test, with 10 min. stress relaxation at intervals of 50% elongation; (b) continuous test.

Table 3
Percentage stress relaxation in various PUs, 10 min after elongation to 300% at a nominal strain rate $3.1\times10^{-2}\,s^{-1}$

| Polymer | PU structure | $\sigma_{300\%}$ (MPa) | Stress relaxation (%) | $E^*_{1H}$ (%) | $E^*_{2H}$ (%) | Residual elongation (%) |
|---|---|---|---|---|---|---|
| PU1 | DBDI–PEA–DEG | 11.3 | 21.0 | 84.4 | 46.5 | 20 |
| PU2 | DBDI–PTHF–DEG | 10.5 | 19.2 | 81.1 | 47.2 | 75 |
| PU9 | DBDI–PEA–BG | 17.2 | 18.6 | 83.3 | 67.7 | 190 |
| PU10 | DBDI–PTHF–BG | 14.0 | 16.8 | 86.9 | 63.0 | 240 |
| PU11 | MDI–PEA–BG | 15.3 | 16.3 | 74.7 | 39.1 | 30 |

Also shown is the initial stress $\sigma_{300\%}$. For comparison, the table also shows the residual elongation and relative hysteresis in first and second cycles of elongation at the same rate $E^*_{1H}$ and $E^*_{2H}$.

[12]. Any adiabatic heating is likely to be absent in interrupted tests, where sufficient time was available for heat to dissipate. As may be seen once again, Figs. 9 and 10 show that, with DBDI as the hard segment, the extent of relaxation is greater than with MDI.

### 3.3. Structural studies

Phase separation, crystallization and orientation phenomena in the present materials were studied by means of wide angle X-ray scattering experiments using Cu $K_\alpha$ radiation, and also DSC, IR dichroism and SEM, from which results are reported elsewhere [1,7].

X-ray diffraction patterns showed significant crystallisability for the PU materials based on DBDI hard segments. There was evidence of the appearance of more or less complete phase separation associated with the formation of discrete crystalline hard domains [7]. However, when the equimolar mixture MDI + DBDI is used for hard segments (PU type C) the crystallinity is considerably reduced [7]. As mentioned elsewhere [1], in the case of PU type D, the degree of crystallinity can be reduced also by employing a more flexible chain extender. Fig. 11 shows example WAXD diffractograms for polyurethanes based on DBDI (with various chain extenders) and MDI. Comparison between curves 2 and 3 illustrates the general point that a DBDI based PU may crystallize, while the corresponding MDI based PU does not. Fig. 11 also shows, however, that crystallinity of the DBDI based PUs is sensitive to the choice of chain extender (Fig. 11, curves 1, 2 and 4). BG and EG lead to distinct diffraction peaks, but DEG gives an amorphous polymer.

It is also noteworthy, however, that the sample preparation technique also influences PU crystallization, as shown for the case of a PU of type D (PU9: DBDI–PEA–BG, $I=110$) in Fig. 12. The crystallinity of PU type D is more pronounced when the polymer is obtained as a sheet cast directly as a melt following synthesis (Fig. 12, curve 1) than when the same PU has been obtained by evaporation

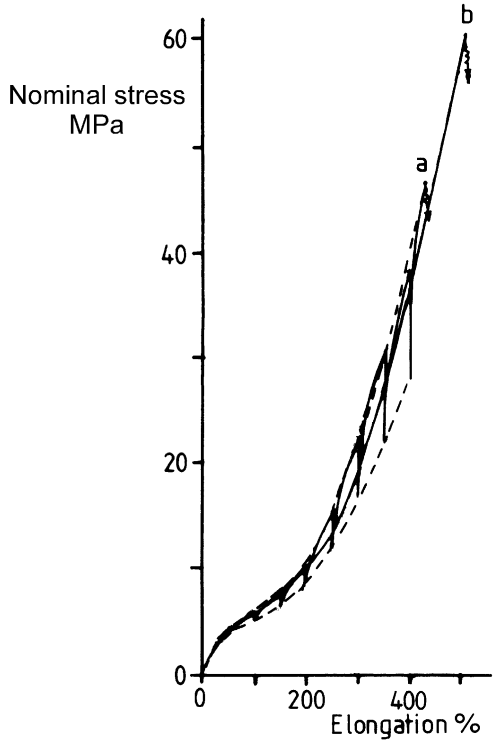


Fig. 10. As Fig. 9 except for type M polymer PU11 (MDI–PEA–BG, $I=110$).

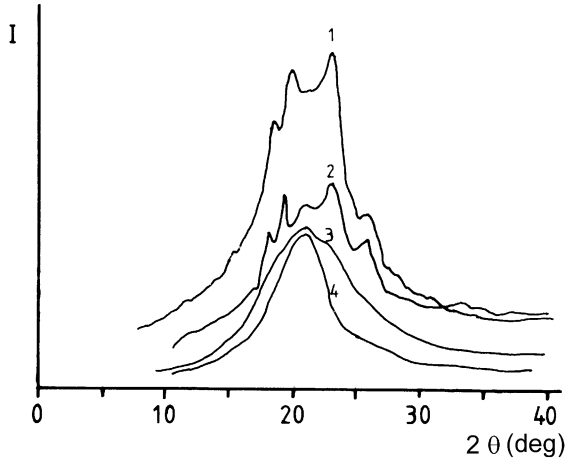


Fig. 11. Wide-angle X-ray diffraction from PUs with DBDI or MDI hard segments and various chain extenders: (1) PU9 (DBDI–PEA–BG, $I=110$); (2) PU12 (DBDI–PEA–EG, $I=110$); (3) PU13 (MDI–PEA–EG, $I=110$); (4) PU6 (DBDI–PEA–DEG, $I=110$).

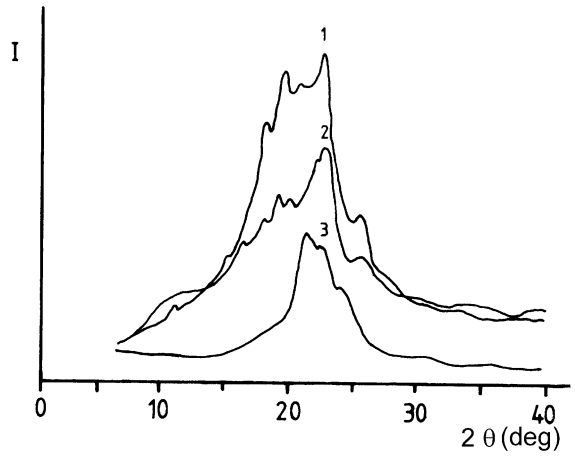


Fig. 12. Wide-angle X-ray diffraction from a PU of type D: PU 9 (DBDI–PEA–BG, $I=110$): (1) PU sheet cast directly from synthesis; (2) PU film obtained by evaporation from 10% solution in DMF; (3) PU film obtained by evaporation, then stretched to 300% elongation, and then released for 24 h (residual elongation 175%); intensity scan perpendicular to the direction of elongation.

from 10% solution of DMF (Fig. 12, curve 2). The crystallinity also changes completely if the solution-cast PU film is stretched to 300% elongation and released (Fig. 12, curve 3).

### 3.4. Interpretation of mechanical response

The general framework of the 'Glass–Rubber' (GR) constitutive model for amorphous polymers [8] provides a convenient means to interpret and explain the variations in mechanical properties reported above. It is based on the fact that, under an imposed isothermal deformation, polymers possess two, and only two, major free energy sinks: (1) perturbation of inter-atom potentials between and within molecules, i.e. what might be called the 'bond-stretching' free energy density $A^{\mathrm{b}}$, and (2) perturbation of conformational entropy, i.e. the 'conformational' free energy density $A^{\mathrm{c}}$. These give rise to two contributions to the Cauchy stress tensor: the bond-stretch contribution $\sigma^{\mathrm{b}}$ and the conformational contribution $\sigma^{\mathrm{c}}$.

The segmented PU elastomers, however, are well-known to be heterogeneous on a length scale of order 10 nm, as a result of phase separation into hard-segment-rich domains and soft-segment-rich domains. In such a case we define a representative length-scale $\Lambda$ ($\gg 10$ nm) beyond which the physical properties can be assumed homogeneous to acceptable accuracy (a reasonable value might be $\Lambda \sim 10$ μm for these materials). In the present work all test specimen dimensions exceeded $\Lambda$. But, in view of the structural inhomogeneity on length-scales below $\Lambda$ but above that of relaxing molecular segments (below which the continuum concept of stress ceases to be meaningful), we recognise that all measured stresses are averages over spatial distributions.

For example, in the limit of complete phase segregation[1], there would be a volume fraction $v_{\mathrm{s}}$ (defined as the 'soft' phase) that is an amorphous polymer above its glass transition, physically crosslinked via its connectivity with the hard phase and entanglements. The part of its free energy contribution $A^{\mathrm{b}}$ associated with shape change would be fully relaxed on the experimental time-scale, and it would respond as a crosslinked elastomer (for the present polymers with isocyanic index $I=110$, we neglect the possibility of entanglement slippage). The remaining 'hard' phase, however, with volume fraction $v_{\mathrm{h}}=1-v_{\mathrm{s}}$, would respond as a glassy or semicrystalline polymer with elastic–viscoplastic character, since we must presume in general that $A^{\mathrm{b}}$ will exhibit rate- and stress-dependent relaxation. In the interpretation that follows we adopt this idealised picture of two distinct phases where the soft phase is elastomeric, and acknowledge the resulting heterogeneity of structure and hence of stress. We employ an overbar to denote volume average stresses, averaged over the representative volume $V=\Lambda^3$.

In view of the above considerations, on length-scales larger than $\Lambda$, equilibrium across any plane dictates that the deviatoric part of the measured Cauchy stress tensor $\mathbf{s}$ may always be expressed as the sum of two terms: the (volume-averaged) conformational stress $\bar{\mathbf{s}}^{\mathrm{c}}$ and the (volume-averaged) bond-stretching stress $\bar{\mathbf{s}}^{\mathrm{b}}$:

$$\mathbf{s} = \bar{\mathbf{s}}^{\mathrm{b}} + \bar{\mathbf{s}}^{\mathrm{c}} \tag{4}$$

and the total measured Cauchy stress is given by

$$\boldsymbol{\sigma} = \bar{\mathbf{s}}^{\mathrm{b}} + \bar{\mathbf{s}}^{\mathrm{c}} - p\mathbf{I} \tag{5}$$

where the mean stress is $-p$, assumed to be determined only by the dilation. Since (we assume) there is complete phase separation, all terms in $\mathbf{s}^{\mathrm{b}}$ vanish within the volume fraction $v_{\mathrm{s}}$ on the experimental time-scale, and $\bar{\mathbf{s}}^{\mathrm{b}}$ is given by an integral over only the hard phase volume $V_{\mathrm{h}}=v_{\mathrm{h}}V$:

$$\bar{\mathbf{s}}^{\mathrm{b}} = \frac{v_{\mathrm{h}}}{V_{\mathrm{h}}} \int_{V_{\mathrm{h}}} \mathbf{s}^{\mathrm{b}} \mathrm{d}V_{\mathrm{h}} \tag{6}$$

Rigorous completion of the model would require knowledge of the relation between phase deformation and macroscopic deformation, but this is unavailable. To proceed, therefore, we employ a gross approximation: we neglect spatial variation of the deformation within the representative volume. We may express this in terms of the deformation gradient $\mathbf{F}$: i.e. the gradient of new particle position $\mathbf{x}$ with respect to original particle position $\mathbf{X}$: $\mathbf{F}=\mathrm{d}\mathbf{x}/\mathrm{d}\mathbf{X}$. If $\mathbf{X}_{\mathrm{h}}$ and $\mathbf{X}_{\mathrm{s}}$ are points within hard and soft domains, respectively, relative to an origin within the representative volume we approximate

[1] This is an ideal case: in practice it is known that different samples of the PU elastomers exhibit differing degrees of soft- and hard-phase segregation, depending on composition and preparation conditions.

$$\mathbf{F}(\mathbf{X}_h) = \mathbf{F}(\mathbf{X}_s) \quad \text{for all } \|\mathbf{X}_h\|,\ \|\mathbf{X}_s\| \le \Lambda \tag{7}$$

This amounts to approximating hard and soft domains as being coupled in parallel.

Consider a uniaxial tensile test parallel to axis 1, say, in which at any instant the axial stretch is $\lambda$ and the rate of stretching is $\dot{\lambda}$: hence $\sigma_{11}=\sigma$, $\sigma_{22}=0$. It follows from Eq. (5) that the applied true stress $\sigma$ may be expressed unambiguously as the sum of two distinct terms:

$$\sigma = \sigma^b + \sigma^c \tag{8}$$

where $\sigma^b = \bar{s}^b_{11} - \bar{s}^b_{22}$ and $\sigma^c = \bar{s}^c_{11} - \bar{s}^c_{22}$. In the idealisations of complete phase separation and parallel coupling between the phases, the contribution $\sigma^b$ is elastic–viscoplastic in character [8], while the contribution $\sigma^c$ is hyperelastic in character. Entanglement slippage is neglected in the present materials prepared with $I=110$, since the molecular length is believed to be sufficient for entanglements to act as physical crosslinks, together with any chemical allophanate crosslinks.

Under these conditions, the contribution $\sigma^c$ $(\lambda)$ will be path-independent, while the elastic–viscoplastic contribution $\sigma^b$ will vary with strain history. Under steady-state flow, however, after completion of the start-up transient, the GR model framework predicts $\sigma^b$ will be a function of only the instantaneous values of $\dot{\lambda}$, $\lambda$ and, in general, the mean stress $-p$. For the present purpose we now neglect the effect of varying mean stress, as the contribution is minor in a uniaxial test [8]. Now consider a load–unload strain cycle, where the magnitude of the rate of stretch is equal and opposite in load and unload portions of the cycle. At a given value of elongation during loading we have $\sigma^b = \sigma^b(+\dot{\lambda}, \lambda)$, whereas at the same elongation during unloading we have $\sigma^b = \sigma^b(-\dot{\lambda}, \lambda)$. But, in view of the associative form of flow rule employed in the model [8], reversing the sign of the rate of stretch will reverse the sign of the deviatoric stresses $\bar{s}^b_{11}$ and $\bar{s}^b_{22}$, from which it follows that

$$\sigma^b(-\dot{\lambda}, \lambda) = -\sigma^b(+\dot{\lambda}, \lambda) \tag{9}$$

This is a useful result, as it means that stress–strain data for load–unload cycles may be used to separate out bond-stretching and conformational contributions to the stress. Thus we may evaluate them as follows, applying Eq. (8) to loading and unloading, and making use of Eq. (9), for any value of elongation where the above restrictions apply (particularly where stress transients can reasonably be neglected):

$$\sigma^c = \frac{1}{2}[\sigma(+\dot{\lambda}, \lambda) + \sigma(-\dot{\lambda}, \lambda)],$$
$$\sigma^b = \frac{1}{2}[\sigma(+\dot{\lambda}, \lambda) - \sigma(-\dot{\lambda}, \lambda)] \tag{10}$$

This separation is illustrated in Fig. 13, for a single load-unload cycle on PU19 to ca 300% elongation, and results of the analysis for materials PU16, PU17 and PU19 are presented in Figs. 14 and 15.

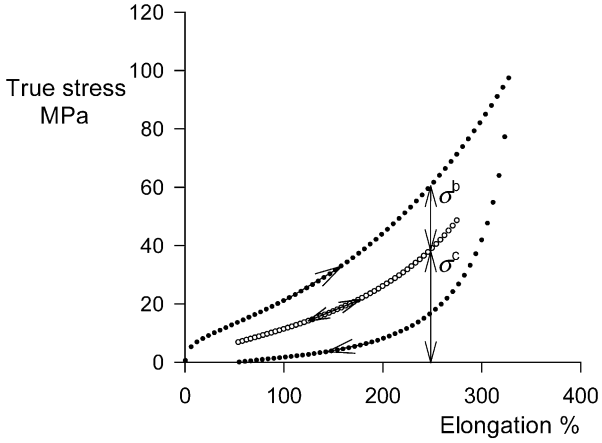


Fig. 13. Apportioning of true stress into contributions from bond-stretching and conformational entropy for polymer PU19, according to Eq. (10).

Fig. 14 shows that the apparent conformational entropy contribution to stress deduced in this way differs little between the three materials. This result is expected, since the soft segment macrodiol employed in all three materials is the same: PTHF. The main difference visible is a slightly smaller stress contribution from the MDI-based polymer, possibly originating in a lower entanglement density in this polymer in view of the lower flexibility of its chains relative to the polymers containing DBDI. By contrast, Fig. 15 shows large differences in the magnitude of the viscoplastic flow stress $\sigma^b$ in the three polymers. The DBDI-based polymer PU16 shows the greatest flow stress, the MDI-based polymer PU17 the lowest, and the DBDI+MDI-based polymer PU19 an intermediate value. These differences may be understood in terms of the crystallinity and more pronounced hydrogen bonding seen in the materials containing DBDI. They provide a common explanation for

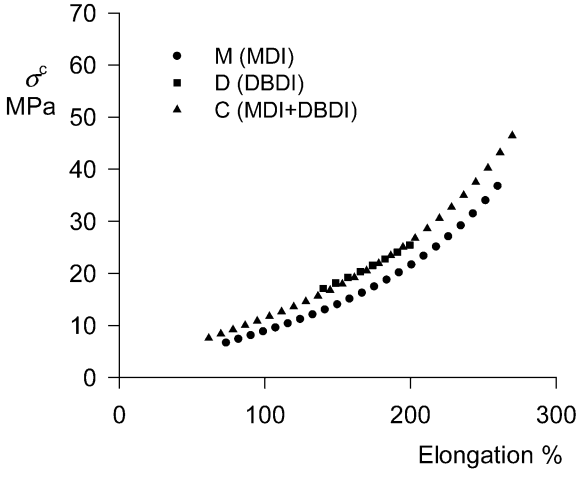


Fig. 14. Conformational entropy contribution to the true stress, $\sigma^c$, as deduced from Eq. (10) from the data shown in Figs. 3–5, for the polymers of type M, D and C.

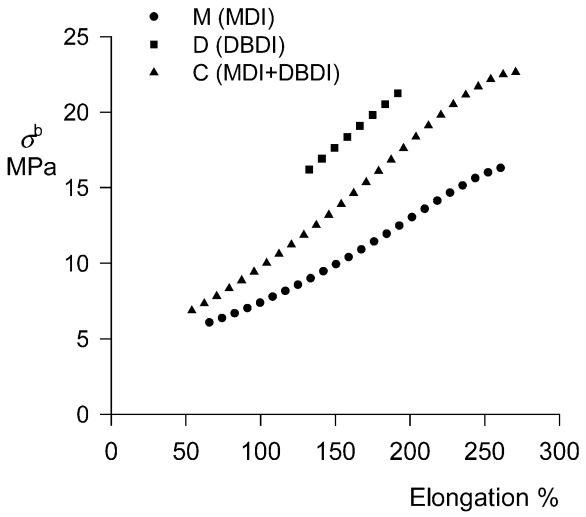


Fig. 15. As Fig. 14, but for the bond-stretching contribution to the stress, $\sigma^b$.

most of the trends in mechanical response discussed above—see below.

Notwithstanding the success of this approach, it is interesting to note that the results in Fig. 15 reveal an inconsistency with the original form of the GR constitutive model. It would predict negative gradients for $\sigma^b(\lambda)$, instead of the positive gradients shown, since the true strain-rate falls with increasing elongation in tests at constant nominal strain-rate. A possible explanation for the discrepancy is that thermally activated flow events in the hard phase are intrinsically anisotropic, whereas the model as previously described assumes they are isotropic [8]. Extension of the GR model to accommodate intrinsic anisotropy, has been discussed in outline [13] and a preliminary discussion of the application to PU elastomers was given before [9]. Further details will be given elsewhere. There could be an alternative explanation: inaccuracy in either or both of the two simplifying assumptions of the model (complete phase separation and parallel phase coupling) is causing the discrepancy. Both would lead to inelasticity in the $\sigma^c$ contribution to stress response, and hence to inaccuracy in the separation in Eq. (10). It is unclear, however, that either could lead to the anomaly seen in Fig. 15.

## 4. Discussion

The primary concern of this paper is the question of how the choice of hard segment composition in PU elastomers affects their mechanical response, especially when the relatively rigid MDI segment is replaced partially or entirely by the relatively more flexible, and crystallisable, DBDI segment. Sections 3.1 and 3.2 reveal a consistent pattern of behaviour. Other parameters being equal, replacement of MDI by DBDI was seen to lead to a response that is substantially stiffer (e.g. higher $E_{1C}$), shows higher hysteresis (e.g. lower $E^*_{1R}$) and lower strain recovery, and higher stress relaxation. The separation of stress into an elastic–viscoplastic component (originating only in the hard phase) and a hyperelastic component as described in the previous section, allows all these results to be explained on a common basis. Applying Eq. (9) to cyclic uniaxial extension at constant elongation rate $\dot{\lambda}$ to a maximum elongation $\lambda_{max}-1$ allows the input strain energy density and recovered energy density to be evaluated:

$$E_{1C} = \int_1^{\lambda_{max}} [\sigma^c(\lambda) + \sigma^b(\dot{\lambda}, \lambda)]\lambda^{-1} d\lambda; \quad E_{1R} = \int_{\lambda_r}^{\lambda_{max}} [\sigma^c(\lambda) - \sigma^b(\dot{\lambda}, \lambda)]\lambda^{-1} d\lambda \tag{11}$$

where $\lambda_r - 1$ is the residual elongation. Suppose that the pattern of behaviour seen in Figs. 14 and 15 were replicated across the range of combinations of PU recipes. It is immediately clear from the dependence of $\sigma^b$ on hard segment content, combined with the relative insensitivity of $\sigma^c$ to the hard segment, that the observed trends in the results for $E_{1C}$ and $E^*_{1R}$ would then be expected from Eq. (11). Similarly, of the two contributions, only $\sigma^b$ is history-dependent. Thus stress relaxation must be attributed to this portion of the stress, and the differences in stress relaxation observed, for example in Figs. 9 and 10, can also be explained in terms of differences in $\sigma^b$ similar to those seen in Fig. 15 (for a different PU recipe).

Thus it is clear that the important effect of inclusion of the DBDI hard segment is to increase the flow stress of the hard phase. This might be considered anomalous in view of the greater conformational mobility of DBDI provided by the $–CH_2–CH_2–$ bridge. The explanation is provided by the structural evidence, revealing more complete phase segregation in the presence of DBDI (other features of the recipe and preparation remaining constant) [7], and in some cases hard phase crystallinity in addition. Closer interactions between the isocyanate groups provided by these structural differences are expected to be associated with a higher density of hard segment hydrogen bonds, leading to a higher stress required to overcome these bonds and achieve plastic flow of the hard phase.

There remain many details in the present results that are not so readily explicable and require further investigation. For example, it was particularly interesting to note that the equimolar mixture MDI+DBDI provided an intermediate case of hard segment, with respect to input and recovered energy (Table 1), but that the residual elongation was less than for both the pure DBDI and pure MDI cases, at least in the cases of PU17 versus PU19 (Fig. 6). A similar feature was present in previous results from a separate series of experiments [7]. This must result from differences in detail between the shapes of the curves of $\sigma^c(\lambda)$ and $\sigma^b(\lambda)$ in the three cases. The present results have also revealed interesting consequences of varying the chain extender

and macrodiol in the PU recipes. These outstanding issues remain as targets for further work.

## 5. Conclusions

A range of novel segmented copolyurethane elastomers has been synthesized, in which the hard segment was the conventional MDI, the more flexible DBDI, or mixtures of the two, and the mechanical responses were investigated. The effects of varying hard segment were studied in the context of a variety of combinations of chain extender, macrodiol and their proportions: a total of 19 formulations. The performance of these materials as elastomers was shown to vary greatly depending on the composition. The most extreme difference between the effects of MDI and DBDI hard segments is seen in the cases where the chain extender-diisocyanate couple is EG–DBDI or BG–DBDI, where the hard segments are observed to crystallise. In such materials the stiffness, hysteresis, residual elongation and stress relaxation are all increased relative to the corresponding MDI based PU. When the couple is DEG–DBDI the same trend is observed, although the differences are less pronounced because the flexible DEG inhibits crystallization. These differences between DBDI and MDI may be attributed to the greater flexibility of DBDI allowing a higher tendency to self-associate by hydrogen bonding. A particularly good balance of elastomeric mechanical properties is observed in the case of PU derived from equimolar mixtures of MDI and DBDI. These polymers are stiffer than those based on pure MDI but show the highest strain recovery of all the systems studied, a primary consideration for elastomers.

Results of the mechanical tests can be understood in terms of a physical model in which the stress is separated objectively into two distinct contributions: an elastic–viscoplastic stress $\sigma^b$ rising from bond-stretching in the hard phase, and a hyperelastic stress $\sigma^c$. This separation has been carried out in the case of the EG–PEA combination and varying DBDI content. The primary effect of the presence of DBDI hard segments was shown to be a substantial increase in $\sigma^b$, for any given elongation, presumably as a result of the closer self-association of hard segments by hydrogen bonding. This single effect of the DBDI is sufficient to explain most of the DBDI-induced differences in the observed mechanical response, across the range of materials studied.

## Acknowledgements

The authors are grateful to the Royal Society for a Joint Project Grant to support the collaboration between Romania and the UK.

## References

[1] Prisacariu Cr. Doctorate Thesis. ‘Gh.Asachi’ University, Iasi, Romania; June 1998.
[2] Prisacariu Cr, Agherghinei I. J Macromol Sci, Pure Appl Chem 2000; A37:785.
[3] Caraculacu A, Petrus A, Geanau L, Fontana I. Romanian Patent RO 56149/1977.
[4] Caraculacu A, Geanau L, Bantas M, Grecu N. ‘Proces tehnologic de fabricare a Moldotanului D’ Institute of Macromolecular Chemistry ‘Petru Poni’ Iasi; 1978.
[5] Saunders JH, Frisch KC. Polyurethanes—chemistry and technology part II. Interscience Publishers: New York; 1964.
[6] Oertel G. Polyurethane handbook. Munich: Hanser Publishers; 1985. p. 570.
[7] Prisacariu C, Olley RH, Caraculacu A, Bassett DC, Martin C. Polymer 2003;44:5407.
[8] Buckley CP, Jones DC. Polymer 1995;36:3301.
[9] Buckley CP, Prisacariu C, Caraculacu A. Euromech Colloquium and Workshop, Vienna; July 2002. p. 96.
[10] Buckley CP, Prisacariu C, Caraculacu A. 12th International conference on deformation, yield and fracture of polymers, Cambridge; April 2003. p. 349.
[11] Abouzahr G, Wilkes GL. Polym Prepr 1980;21:193.
[12] Buckley CP. Experimental methods for rubberlike solids. In: Saccommandi G, Ogden RW, editors. Mechanics and thermomechanics of rubberlike solids—CISM Courses and Lectures No.452. Vienna: Springer; 2004.
[13] Buckley, CP, Wu, JJ. 19th Annual meeting of the polymer processing society, Melbourne; July 2003.